**ENGINEERING MECHANICS 2009**
National Conference with International Participation
Svratka, Czech Republic, May 11 – 14, 2009

**pp. 413–424**
Paper **#132**

# COMPARISON OF NUMERICALLY SIMULATED PRESSURE ON THE SURFACE OF A FLUTTERING PROFILE WITH EXPERIMENT IN WIND TUNNEL

**J. Horáček[*], P. Sváček[**], V. Vlček[*], M. Feistauer[***]**

**Summary:** *The paper compares original experimental results with numerical solution of a 2D aeroelastic problem. The incompressible turbulent flow over a freely vibrating airfoil, with two degrees of freedom for rotation and translation with large vibration amplitudes, is described by the Reynolds averaged Navier-Stokes (RANS) equations written in Arbitrary Lagrangian-Eulerian (ALE) form. The Spalart-Allmaras turbulence model is used. The flow is solved by the stabilized finite element method. The numerical results are compared with the optical measurements of flow field around a fluttering double circular arc (DCA) 18% profile elastically supported in a subsonic wind tunnel. The interferometry method was used for airflow visualization in different phases of the profile motion. The numerical results for the pressure on the profile surface are in good agreement with the measurement.*

## 1. Introduction

In many technical disciplines the interaction of fluid flow and a vibrating structure plays an important role, see, e.g., Dowell (1995). During last years, significant advances have been made in the development of computational methods for simulation of the fluid-structure interaction, see, e.g., Bathe (2007). In the present study the main attention is paid to the comparison of numerical simulations of self-sustained vibrations of a profile in turbulent incompressible flow with the experimental results. The mathematical analysis consists of the fluid flow 2D model in interaction with a flexibly supported profile, which can vibrate vertically and rotate around its elastic axis.

The numerical solution of RANS equations is carried out with the use of the finite element method (FEM) for the spatial discretization of the problem. The finite elements for velocity and pressure were selected to satisfy the Babuška-Brezzi condition in order to guarantee the stability of the scheme. The stabilization based on GLS (Galerkin Least-Squares) method together with div-div stabilization was employed in order to suppress the appearance of spurious oscillations due to very high Reynolds numbers. The choice of the stabilization parameters is based on the numerical analysis of the problem as well as the numerical

[*] Ing. Jaromír Horáček, DrSc., Ing. Václav Vlček, CSc., Institute of Thermomechanics, Academy of Sciences of the Czech Republic, Dolejškova 5, 182 00, Praha 8, Czech Republic
[**] Mgr. Petr Sváček, PhD, Czech Technical University Prague, Faculty of Mechanical Engineering, Karlovo nám. 13, 121 35 Praha 2, Czech Republic
[***] prof. Miloslav Feistauer, DrSc., Charles University Prague, Faculty of Mathematics and Physics, Sokolovská 83, 186 75 Praha 8, Czech Republic

experience, see Sváček et al. (2007) and Lube (1994). The Spalart-Allmaras turbulence model is approximated by the FEM stabilized by the streamline upwind/Petrov-Galerkin (SUPG) method.

The original measurement was performed in a wind tunnel for the airflow velocity higher than the critical flow velocity for loss of the profile stability by flutter, thus the vibration amplitudes were large, see Vlček et al. (2008). The images of the flow field were recorded for prescribed phase delays during one oscillation period of the profile from which the pressure on the vibrating surface was evaluated at given time instants.

## 2. Mathematical fluid flow model

The character of the flow depends on the magnitude of the Reynolds number. For a sufficiently small Reynolds number the flow is laminar but with increasing Reynolds numbers it becomes turbulent. The turbulent incompressible flow can be modelled by the Reynolds Averaged Navier-Stokes (RANS) equations

$$\begin{aligned} \frac{\partial V_i}{\partial t} - \sum_{j=1}^{2} \frac{\partial}{\partial x_j} \nu \left( \frac{\partial V_i}{\partial x_j} + \frac{\partial V_j}{\partial x_i} \right) + \sum_{j=1}^{2} \frac{\partial}{\partial x_j} \left( V_j V_i \right) + \frac{\partial P}{\partial x_i} = -\sum_{j=1}^{2} \frac{\partial R_{ij}}{\partial x_j}, \qquad i = 1,2, \\ \sum_{i=1}^{2} \frac{\partial V_i}{\partial x_i} = 0, \end{aligned} \tag{1}$$

where $\mathbf{V} = \left( V_1, V_2 \right)$ is the mean value of the fluid velocity, $\nu$ is the kinematic fluid viscosity, $P$ is the mean value of the kinematic pressure (i.e., pressure $p$ divided by the fluid density $\rho$), the terms $R_{ij}$ are the Reynolds stresses expressed in the form

$$R_{ij} = \nu_T \left( \frac{\partial V_i}{\partial x_j} + \frac{\partial V_j}{\partial x_i} \right), \tag{2}$$

and $\nu_T$ is a turbulent viscosity.

The value of $\nu_T$ can be either obtained by the solution of one or more partial differential equations for additional quantities – see Wilcox (1993).

In order to numerically simulate aeroelastic problems for large vibration amplitudes the ALE formulation of Reynolds equations and of the turbulence model needs to be introduced. Following the notation in Dubcová et al. (2008), we can rewrite the Reynolds Averaged Navier-Stokes equations in the ALE form as

$$\begin{aligned} \frac{\mathrm{D}^{\mathcal{A}_t} V_\mathrm{i}}{\mathrm{D}t} - \sum_{\mathrm{j}=1}^{2} \left[ \frac{\partial}{\partial x_\mathrm{j}} \left( \nu + \nu_\mathrm{T} \right) \left( \frac{\partial V_\mathrm{i}}{\partial x_\mathrm{j}} + \frac{\partial V_\mathrm{j}}{\partial x_\mathrm{i}} \right) \right] + \left( \left( \mathbf{V} - \mathbf{w_g} \right) \cdot \nabla \right) V_\mathrm{i} + \frac{\partial P}{\partial x_\mathrm{i}} = 0, \qquad i = 1,2, \\ \sum_{\mathrm{i}=1}^{2} \frac{\partial V_\mathrm{i}}{\partial x_\mathrm{i}} = 0, \end{aligned} \tag{3}$$

where $\dfrac{\mathrm{D}^{\mathcal{A}_t}}{\mathrm{D}t}$ denotes the ALE derivative and $\mathbf{w_g}$ is the domain velocity. System (3) is considered in a time-dependent domain $\Omega_t$. The symbol $\mathcal{A}_t$ denotes a regular one-to-one Arbitrary Lagrangian-Eulerian (ALE) mapping of the reference configuration $\Omega_0$ onto the current configuration $\Omega_t$ for any time instant $t \in [0,T]$ - see Nomura & Hughes (1992).

The system of equations (3) is equipped with suitable boundary and initial conditions (see Fig.1). On the moving part of boundary (airfoil surface $\Gamma_{Wt}$) the kinematic boundary condition is prescribed, i.e. $\mathbf{V} = \mathbf{w}_g$ on $\Gamma_{Wt}$. At the inlet and on the fixed impermeable channel walls $\Gamma_D$ the Dirichlet conditions $\mathbf{V} = \mathbf{V}_D$ are considered and at the outlet the condition:

$$-(\nu+\nu_T)\sum_{j=1}^{2}\left(\frac{\partial V_i}{\partial x_j}+\frac{\partial V_j}{\partial x_i}\right)n_j+\left(P-P_{ref}\right)n_i=0 \quad \text{on } \Gamma_O, \quad i=1,2\ , \tag{4}$$

where $\mathbf{n}=(n_1,n_2)$ is the unit normal to the boundary $\partial\Omega_t$ of the domain $\Omega_t$, $\Gamma_O$ is the outlet and $P_{ref}$ denotes a prescribed reference outlet pressure. The initial condition $\mathbf{V}(x,0)=\mathbf{V}_0(x), \quad x\in\Omega_0$ is considered.

The turbulent viscosity is determined with the aid of the Spalart-Allmaras turbulence model. It can be written in the ALE form (see Wilcox,1993):

$$\frac{\mathrm{D}^{A_t}\tilde{\nu}}{\mathrm{D}t}+\left(\left(\mathbf{V}-\mathbf{w}_g\right)\cdot\nabla\right)\tilde{\nu}=\frac{1}{\beta}\left[\sum_{i=1}^{2}\frac{\partial}{\partial x_i}\left(\left(\nu+\tilde{\nu}\right)\frac{\partial\tilde{\nu}}{\partial x_i}\right)+c_{b_2}\left(\nabla\tilde{\nu}\right)^2\right]+G-Y \qquad \text{in } \Omega_t \tag{5}$$

for an additional quantity $\tilde{\nu}$ and equipped with the boundary condition $\tilde{\nu}=0$ on $\Gamma_{Wt}$ and $\partial\tilde{\nu}/\partial\mathbf{n}=0$ on $\Gamma_O\cup\Gamma_D$.

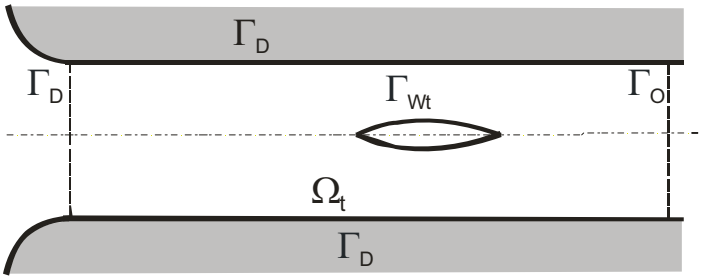


Figure 1 Scheme of the computational region around the vibrating airfoil in the channel.

The turbulent viscosity $\nu_T$ is defined as

$$\nu_T=\tilde{\nu}\frac{\chi^3}{\chi^3+c_v^3}, \qquad \chi=\frac{\tilde{\nu}}{\nu}. \tag{6}$$

The functions $G$ and $Y$ are functions of the tensor of rotation of the mean velocity and depend on the wall distance $y$:

$$G=c_{b_1}\tilde{S}.\tilde{\nu}, \qquad Y=c_{w_1}\frac{\tilde{\nu}^2}{y^2}\left(\frac{1+c_{w_3}^6}{1+c_{w_3}^6/g^6}\right)^{\frac{1}{6}},$$

$$\tilde{S}=\left(S+\frac{\tilde{\nu}}{\kappa^2y^2f_{v_2}}\right), \qquad f_{v_1}=\frac{\chi^3}{\chi^3+c_v^3}, \qquad f_{v_2}=1-\frac{\chi}{1+\chi f_{v_1}}, \qquad g=r+c_{w_2}\left(r^6-r\right),$$

$$r=\frac{\tilde{\nu}}{\tilde{S}\kappa^2y^2}, \qquad S=\sqrt{2\sum_{i,j}\omega_{ij}}, \qquad \omega_{ij}=\frac{1}{2}\left(\frac{\partial V_i}{\partial x_j}-\frac{\partial V_j}{\partial x_i}\right). \tag{7}$$

The following choice of constants is used:

$$c_{b_1} = 0.1355, \qquad c_{b_2} = 0.622, \quad \beta = 2/3, \qquad c_{v} = 7.1, \qquad c_{w_2} = 0.3,$$

$$c_{w_3} = 2.0, \qquad \kappa = 0.41, \quad c_{w_1} = c_{b_1} / \kappa^2 + \left(1 + c_{b_2}\right) / \beta . \tag{8}$$

## 3. Structural model

The profile can vertically vibrate with the displacement $h(t)$ and rotate around the elastic axis EA with the rotation angle $\alpha(t)$. Fig. 2 shows the elastic support of the profile on translational and rotational springs with a bending stiffness $k_{\mathrm{h}}$ and torsion stiffness $k_{\alpha}$. The pressure and viscous forces acting onto the vibrating profile immersed in the flow result in the aerodynamic lift force $L(t)$, the torsional moment $M(t)$ the drag force $D(t)$ defined by

$$L = -l \int_{\Gamma_{\mathrm{Wt}}} \sum_{\mathrm{j}=1}^{2} \tau_{2\mathrm{j}} n_{\mathrm{j}} \mathrm{d}S, \qquad M = l \int_{\Gamma_{\mathrm{Wt}}} \sum_{\mathrm{ij}=1}^{2} \tau_{\mathrm{ij}} n_{\mathrm{j}} r_{\mathrm{i}}^{\mathrm{ort}} \mathrm{d}S, \qquad D = -l \int_{\Gamma_{\mathrm{Wt}}} \sum_{\mathrm{j}=1}^{2} \tau_{\mathrm{i}} n_{\mathrm{j}} \mathrm{d}S, \tag{9}$$

where

$$\tau_{\mathrm{ij}} = \rho \left[ -p\delta_{\mathrm{ij}} + \left(\nu + \nu_{\mathrm{T}}\right) \left( \frac{\partial V_{\mathrm{j}}}{\partial x_{\mathrm{j}}} + \frac{\partial V_{\mathrm{j}}}{\partial x_{\mathrm{j}}} \right) \right], \qquad r_1^{\mathrm{ort}} = -\left(x_2 - x_{\mathrm{EA2}}\right), \qquad r_2^{\mathrm{ort}} = +\left(x_1 - x_{\mathrm{EA1}}\right). \tag{10}$$

By $\tau_{\mathrm{ij}}$ we denote the components of the stress tensor, $\delta_{\mathrm{ij}}$ denotes the Kronecker symbol, $\mathbf{n} = \left(n_1, n_2\right)$ is the unit outer normal to $\partial\Omega_{\mathrm{t}}$ on $\Gamma_{\mathrm{Wt}}$ (pointing into the profile) and $x_{\mathrm{EA}} = \left(x_{\mathrm{EA1}}, x_{\mathrm{EA2}}\right)$ is the position of the elastic axis EA. Relations (8) and (9) define the coupling of the fluid model with the structural model.

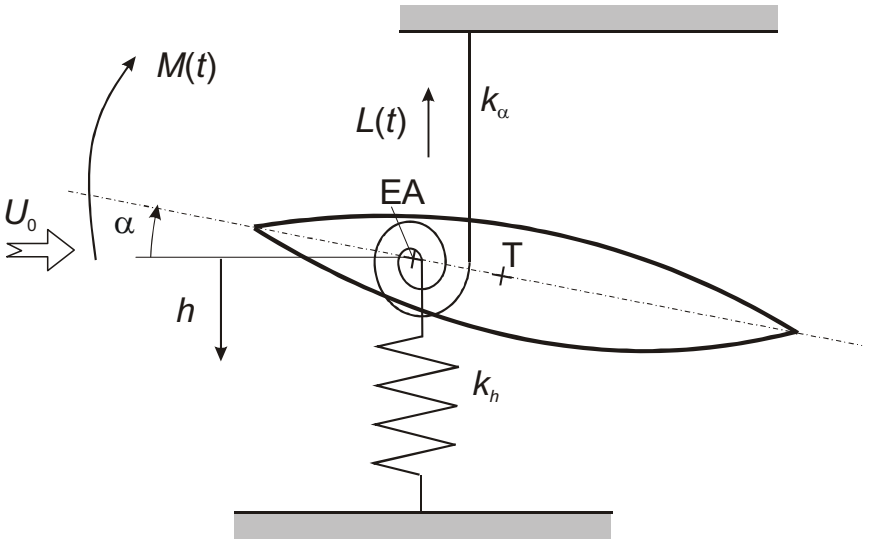


Figure 2 Scheme of the elastic support of the airfoil on translational and rotational springs.

## 4. Numerical approximation of the flow problem

In order to solve the problem numerically, we start from the time discretization of the flow model. The ALE derivative is approximated by a two step backward difference formula. The problem discretized in time is solved by the finite element method. The construction of the finite element space is based on a triangulation $\mathcal{T}_\Delta$ of a polygonal approximation $\Omega$ of the computational domain $\Omega_t$ at time $t$.

In the finite element solution of incompressible Navier-Stokes equations several important obstacles need to be overcome. First, it is necessary to take into account that the finite element velocity/pressure pair has to be suitably chosen in order to satisfy the Babuška-Breezi condition, which guarantees the stability of the scheme – see, e.g., Girault and Raviart (1986). In practical computations, the finite element spaces are defined over a triangulation $K \in \mathcal{T}_\Delta$, formed by a finite number of closed triangles $K \in \mathcal{T}_\Delta$. In our computations, the well-known Taylor-Hood P2/P1 conforming elements are used for the velocity/pressure approximation. This means that the finite element approximation of the pressure $p_\Delta$ is a piecewise linear function and the approximation of the velocity $\mathbf{v}_\Delta$ is a piecewise quadratic vector-valued function.

The standard Galerkin discretization may produce approximate solutions suffering from spurious oscillations for high Reynolds numbers. In order to avoid this drawback, the stabilization via streamline-diffusion/Petrov-Galerkin technique is applied, see, e.g., Gelhard et al. (2005), Sváček et al. (2007). Moreover, it is necessary to design carefully the computational mesh, using adaptive grid refinement in order to allow an accurate resolution of time oscillating thin boundary layers, wakes and vortices. We use the anisotropic mesh adaptation technique by Dolejší (2001) for the construction and adaptive refinement of the mesh.

The nonlinear Spalart-Allmaras equation (5) is discretized by piecewise linear elements. In order to guarantee the positivity of the function $\tilde{\nu}$ needs to preserve, the SUPG/GLS stabilization applied as in Sváček et al. (2007). However, the use of SUPG/GLS stabilization still does not avoid local oscillations near sharp layers, which can lead to pathological situations with negative viscosity. In order to solve this problem, the additional artificial viscosity stabilizing procedure based on crosswind diffusion is introduced, cf. Codina (1993).

## 5. Measurement set - up

For simultaneous measurement of the periodic profile vibrations and the optical measurement of unsteady high speed airflow, a method of phase shift was used. The measurement of flow fields in selected phases of the oscillation period was carried out. An arbitrary periodic quantity is possible to choose for controlling the image record triggering in a given phase. The pulse source of the light and the digital camera was synchronized with the selected phase of the vertical position of the profile. Using this method, the relations among the unsteady flow field, the profile motion and the aerodynamic forces loading the vibrating body can be determined in selected phases of the periodic motion.

Vacuum subsonic wind tunnel was used for the experiments, see Fig.3. The double circular arc (DCA) 18% profile with the chord length $b$=120 mm and thickness 21.6 mm was elastically supported in the test section of the wind tunnel. The test section was 80 mm wide and 210 mm high. Centre of rotation (EA) of the profile was at 1/3 of the chord behind the leading edge, for more details on the measurement see Vlček et al. (2008).

Experimentally established eigenfrequencies $f_1$ and $f_2$ and damping of the system for zero airflow velocity are presented in Table I. By increasing the velocity both frequencies converge to the flutter frequency 20.4 Hz at the critical velocity at about Mach number $M$=0.38 (Reynolds number Re=1.04 x $10^6$). Above this velocity, the system became unstable by flutter with a rapid increase of vibration amplitudes and the self-excited motion of the profile in a limit cycle oscillation.

| Mode No | Natural frequency | Damping ratio | Mode shape |
|---|---|---|---|
| 1 | 18.38 [Hz] | 3.22 [%] | translation |
| 2 | 38.13 [Hz] | 0.96 [%] | torsion |
| 3 | 146.9 [Hz] | 0.72 [%] | parasitic |

Table I Dynamic characteristics of the model.

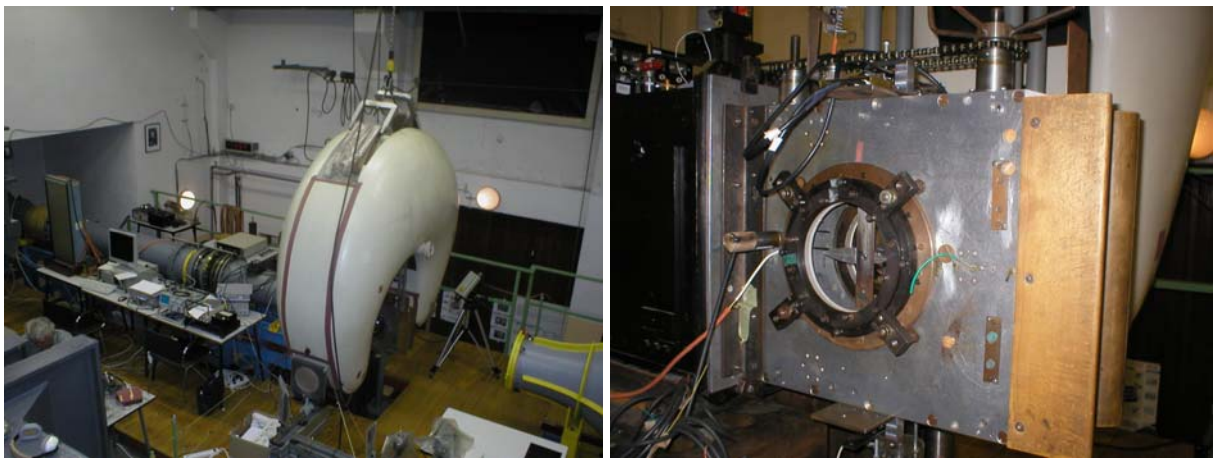

(a) (b)

Figure 3 (a) Wind tunnel with Mach-Zehnder interferometer, (b) test section with the DCA profile.

## 6. Flow measurement by interferometry method

The flow field in the vicinity of the profile was measured by interferometry method at the inflow velocity $M$=0.38, which is slightly above the flutter stability of the profile. The vibration amplitudes were relatively large, up to about 6 mm of the peak-to-peak values for vertical translation $h$ and 9 degrees for peak-to-peak values of the rotation angle $\alpha$ around the elastic axis. Individual phases of one oscillation cycle are documented in Fig. 4 at the 16$^{th}$ time instants. Exposition of each photograph was performed with the time delay approximately of 4 s. This time was required for the recharging of electrical condensers of the flash apparatus.

Translational and rotational displacements of the profile evaluated from the photos in Fig. 4 taken in the selected 16$^{th}$ phases $\varphi \in \langle 0, 2\pi \rangle$ during one cycle of the self-oscillations are shown in Fig. 5. It can be concluded that the rotation and translation of the profile were nearly in phase. However, the system behavior was asymmetric, the downward vertical displacement and negative (counterclockwise) direction of the rotation prevailed. The reason for it can be in

a small asymmetry of the profile construction including an asymmetry in the profile installation in the wind tunnel test section.

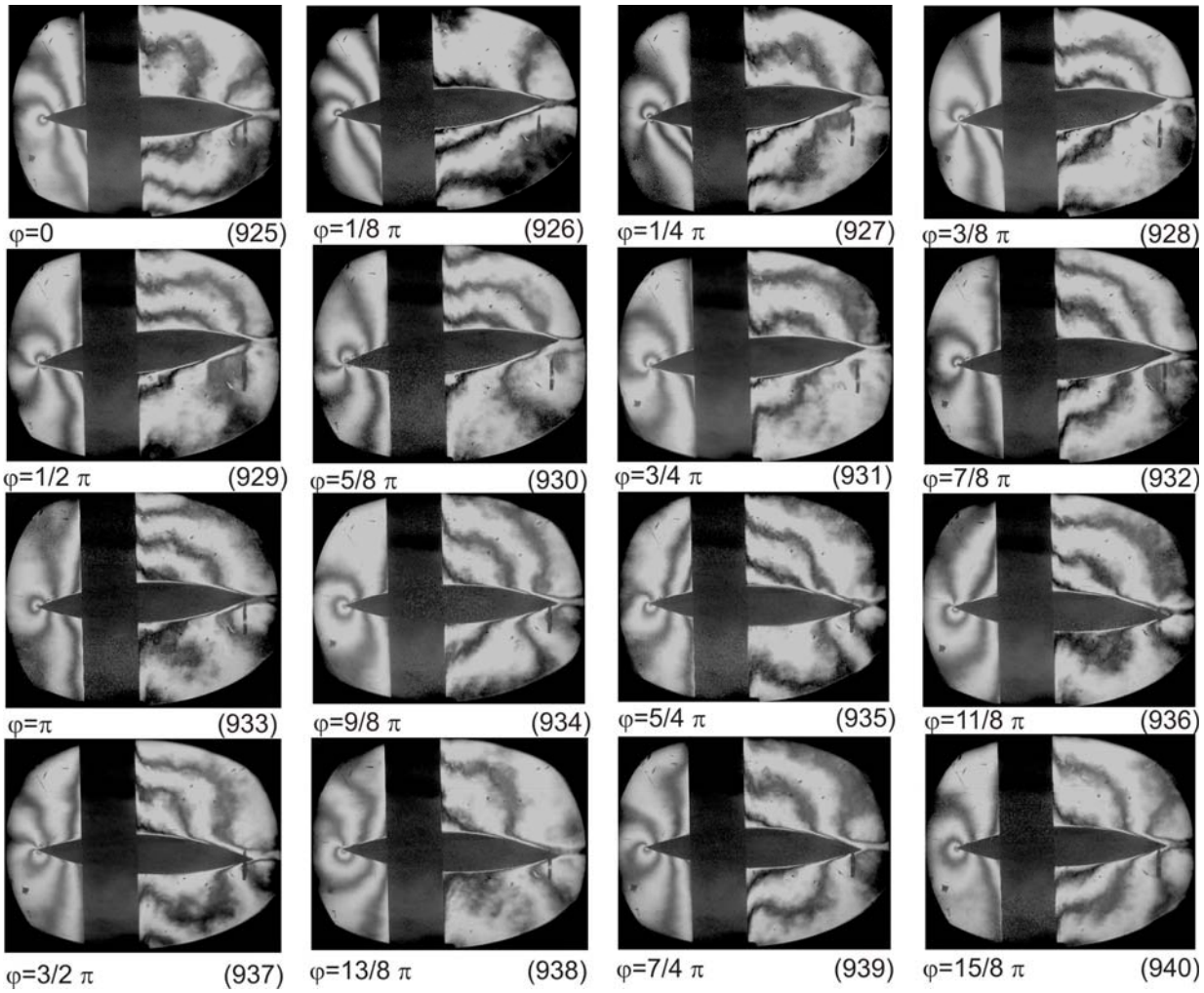


Figure 4 Interferograms (No 925-940) of the flow field around vibrating DCA profile for one period of the self-oscillations after the lost of stability by flutter in 16th motion phases $\varphi$.

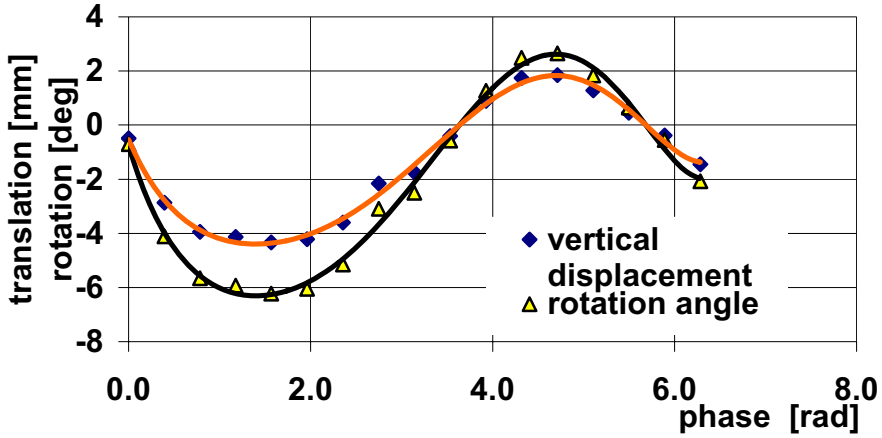


Figure 5 Angle of attack and vertical translation of the profile during one period of the self-excited airfoil motion in 16th motion phases $\varphi \in < 0, 2\pi >$.

## 7. Results and discussion

The pressure on the moving profile surface was numerically simulated for the prescribed airfoil motion given by the attack angle $\alpha$ and vertical translation $h$ of the elastic axis (see Fig. 6) corresponding to the measured self-vibration regime in Fig. 5. The oscillation frequency was 20.4 Hz, the angle $\alpha$ varied from -6° to + 3° and the translation $h$ from –4 mm to +2 mm. The oncoming airflow velocity $U_0$=130 m/s, air density $\rho = 1.225$ kg/m$^3$, kinematic viscosity $\nu$ =1.5 x 10$^{-5}$ m/s$^2$ and the total pressure in the oncoming flow $p_0$=9 761.8 Pa (approximately equal to the atmospheric pressure) were considered in the numerical computations.

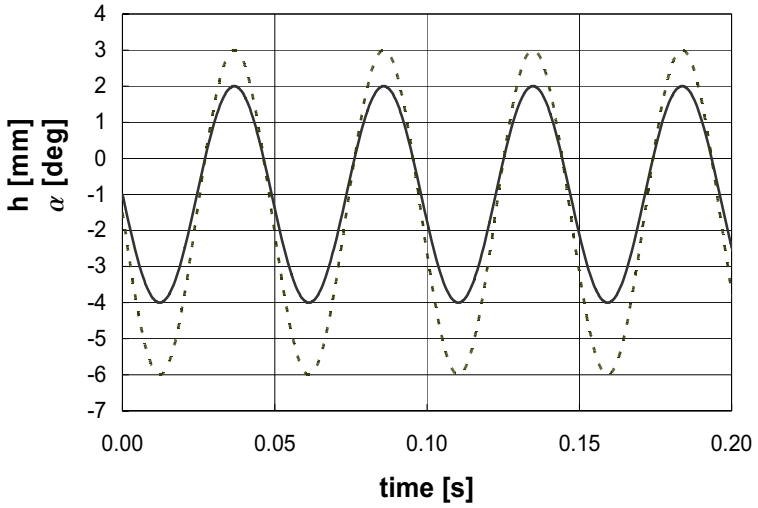


Figure 6 Prescribed periodic vibrations of the profile by angle of attack $\alpha$ (dashed line) and vertical translation $h$ (full line) following the measured self-excited airfoil motion.

The pressure was evaluated from the interferograms using the method of infinite-fringe mode and assuming isentropic flow. The accuracy of the pressure evaluation was decreased by a small depth of the measurement test section (80 mm) in the wind tunnel, and therefore only 18.3 fringes covered the whole range of the subsonic airflows velocities. Moreover, a substantial part of field of view of the width 30 mm (i.e. ¼ of the profile chord) was hidden behind a supporting strap flexibly fixing the airfoil in the measurement section. An interpolation of the interferometry fringes, partly hidden in the non-visible region of the flow field covered by the metal strap carrying the profile, was problematic. From this reason, only midpoints of the black and white fringes were used for calculation of the pressure on the airfoil surface. In this way one interference fringe (i.e., one pair of the white and black fringe) corresponded to the change of the airflow velocity about 15 m/s (i.e., the change in the Mach number about 0.05). In the leading edge of the profile it was also difficult to evaluate the pressure with a better accuracy, because of the fringes in this part of the profile have a very high density and the fringes are not clearly distinguishable one from the other.

The dimensionless pressure $p/p_0$ computed on the profile upper and lower surfaces in the 16$^{th}$ phases of one vibration period is presented in Fig. 7 together with the pressures evaluated from the interferograms No 925–940 presented in Fig. 4.

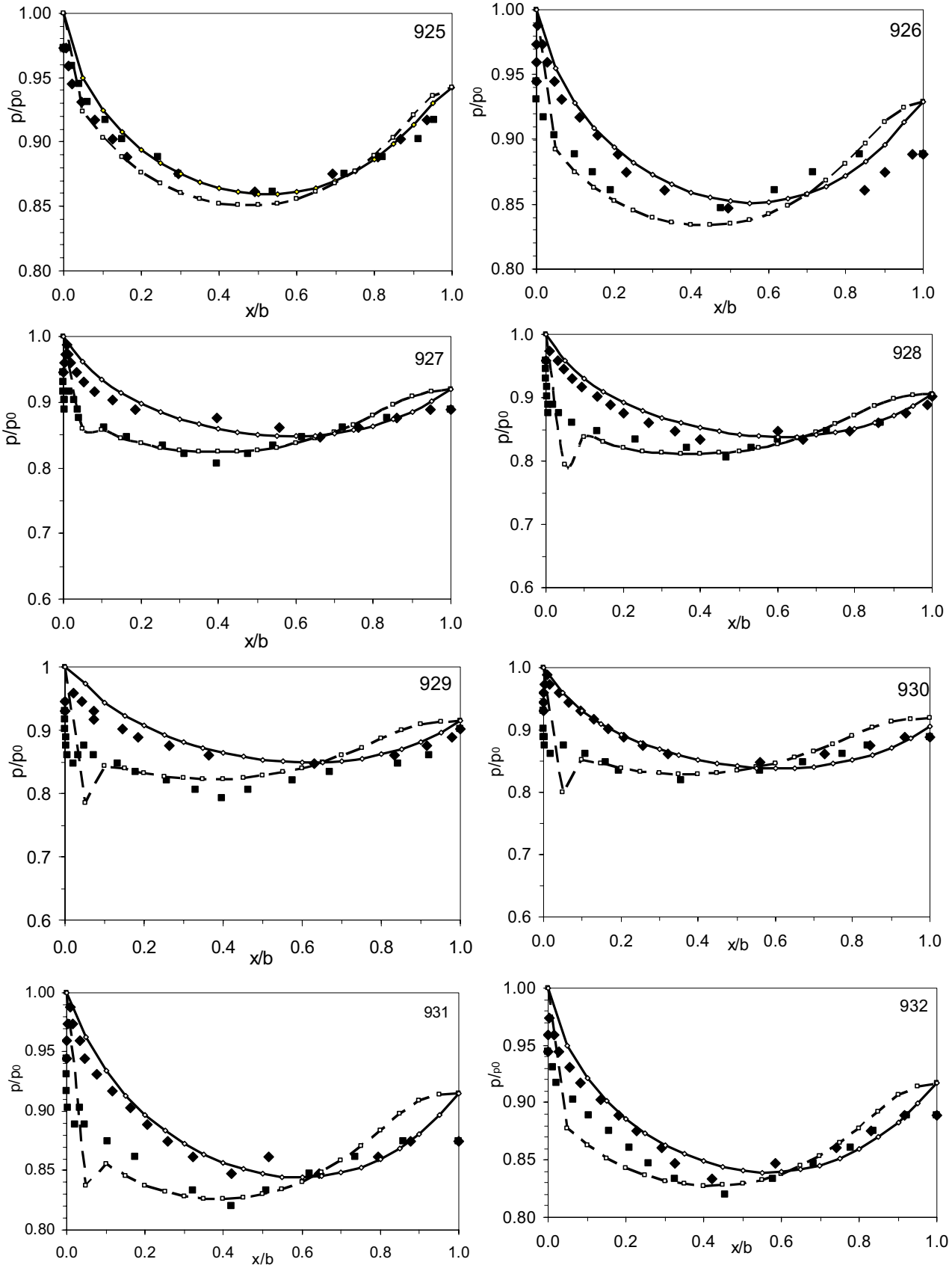


Figure 7 Pressure on the vibrating airfoil during one period: a/ experiment – on upper (♦) and lower (■) surfaces, b) computed - upper (full line) and lower (dashed line) surfaces.

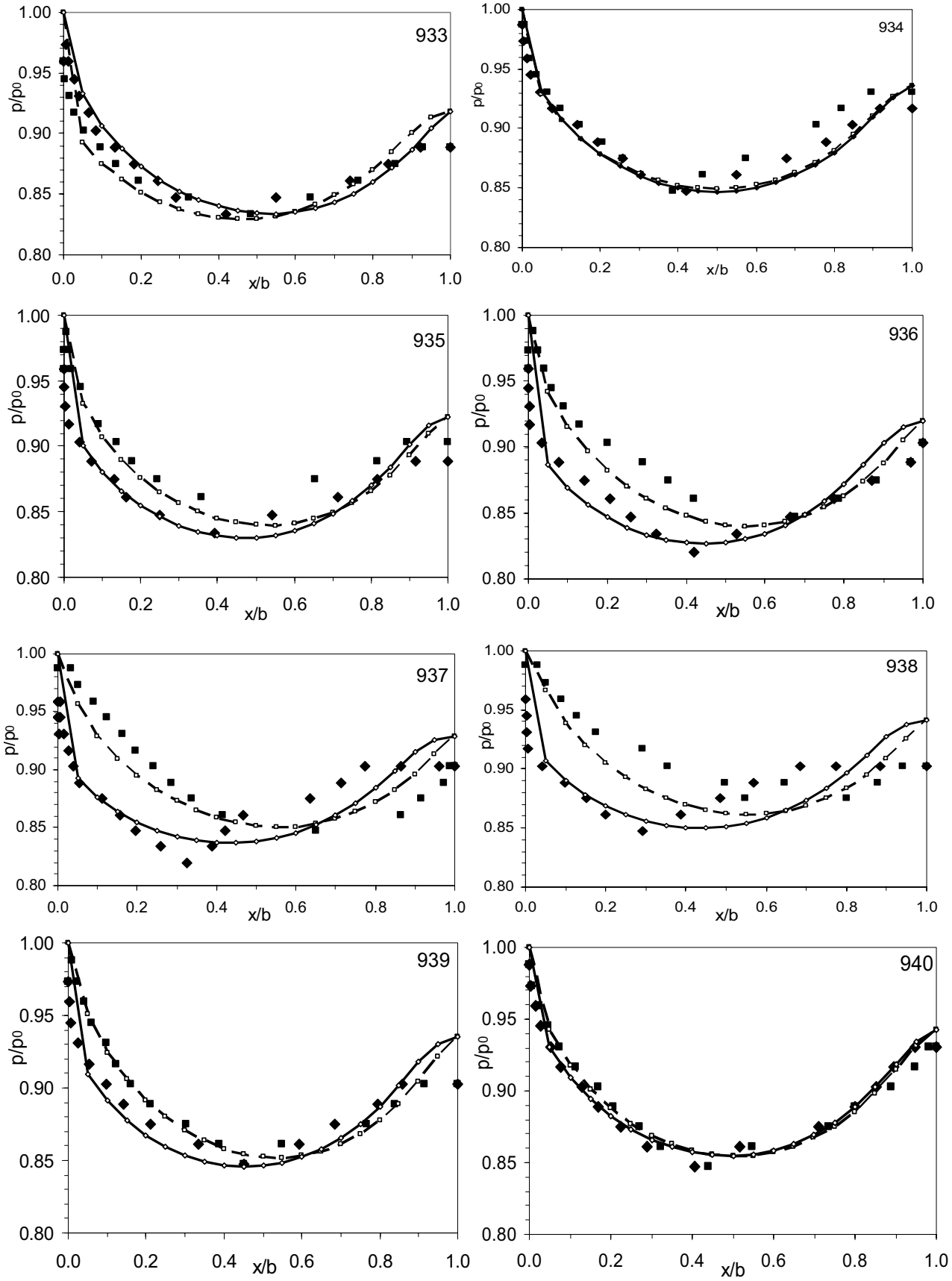


Figure 7 – continued. (The numbers 925–940 correspond to the interferograms in Fig. 4.)

For the negative attack angles ($\alpha < 0$ – see the interferograms No 926–933) and the leading part of the profile ($x/b < 0.5$) the pressure has higher values on the upper profile surface than on the lower surface. It is changed in the trailing part of the profile ($x/b > 0.5$), where the higher pressure is on the lower surface.

For higher negative angles of attack ($\alpha << 0$), especially for the interferograms No 929–930, the graphs for the pressure computed on the lower side of the profile at the nose near the distance $x/b \cong 0.05$ from the very sharp leading edge are not smooth due to a local flow separation. For the positive angles of attack ($\alpha>0$ see the interferograms No 935–939) no flow separation region is possible to detect in the computed pressures, and the scheme of the pressure interchanges along the upper and lower surfaces is opposite in comparison to the cases $\alpha < 0$ mentioned above. Near an equilibrium profile position ($\alpha \cong 0$ - see the interferograms No 925 and 940) the pressure on the upper and lower surfaces is approximately the same. In general, the higher flow velocity outside the boundary layer is associated with the smaller pressure on the surface of the profile. At the trailing edge of the profile the computed pressure is usually higher than the pressure evaluated from the interferograms.

Taking into account the above-mentioned problems with the evaluation of the interferograms, the agreement of the computed and measured pressure on the profile is good.

Fig. 8 shows the comparison of the computed lift force $L$ given by integration of the pressure around the profile surface with the lift force evaluated from the experimentally obtained pressure distribution along the upper and lower surfaces of the profile.

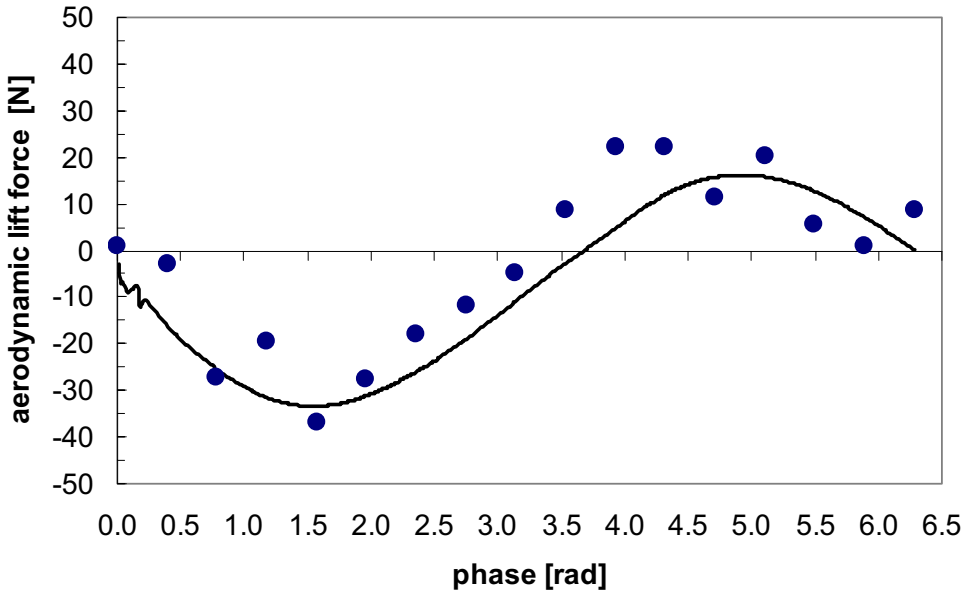


Figure 8 Resulting measured and computed (full line) aerodynamic lift force $L$ loading the profile during one period of the self-excited airfoil motion.

## 8. Conclusions

Aeroelastic model with a double arc circle profile was investigated in wind tunnel in the regime of flutter instability at the Mach number $M$=0.38. Interferometry was used for visualization of the airflow around the vibrating profile during the whole oscillation cycle, which was divided into 16 phases. From the interferograms, the pressure distribution on the

profile was determined. The accuracy of the evaluation was decreased due to the necessity of extrapolation of interferometry fringes in the part of the test section, where the flow field was shielded by the support construction of the model, and where the flow field was not visible. The method developed for the numerical simulation of airfoil aeroelastic behaviour in turbulent flow was successfully validated by experimental data for prescribed airfoil vibration for flow velocities above the instability threshold for flutter.

## 9. Acknowledgement

The research was supported by the project of the Grant Agency of the Czech Republic by the project No. 101/09/1522 "*Experimental research of unsteady flow patterns around vibrating airfoil with application in aeroelasticity*".

## 10. References

Bathe, K.J. (ed.) (2007) *Computational Fluid and Solid Mechanics*. Elsevier.

Codina, R. (1993) A discontinuity capturing crosswind-dissipation for the finite element solution of the convection diffusion equation. *Comput. Methods Appl. Mech. Engrg*, 110, pp. 325-342.

Dolejší, V. (2001) Anisotropic mesh adaptation technique for viscous flow simulation. *East-West Journal of Numerical Mathematics*, 9:1–24.

Dowell, E.H. (1995) *A Modern Course in Aeroelasticity*. Kluwer Academic Publishers, Dodrecht.

Dubcová, L., Feistauer, M., Horáček, J. & Sváček, P. (2008) Numerical simulation of airfoil vibrations induced by turbulent flow. *J. Comput. and Appl. Math*., 218(1):34-42.

Gelhard, T., Lube, G., Olshanskii, M. A. & Starcke, J.H. (2005) Stabilized finite element schemes with LBB-stable elements for incompressible flows. *J. Comput. and Appl. Math*., 177:243–267.

Girault, V. & Raviart, P.A. (1986) *Finite Element Methods for the Navier-Stokes Equations*. Springer-Verlag, Berlin.

Lube, G. (1994) Stabilized Galerkin finite element methods for convection dominated and incompressible flow problems. *Num. Anal. and Math. Model.*,Banach Center publications 29, pp. 85–104.

Nomura, T. & Hughes, T.J.R. (1992) An arbitrary Lagrangian-Eulerian finite element for interaction of fluid and a rigid body. *Comput. Methods in App. Mech. Engrg*, 95, pp. 115-138.

Sváček, P., Feistauer, M. & Horáček, J. (2007) Numerical simulation of flow induced airfoil vibrations with large amplitudes. *J. Fluids and Structures*, 23, pp. 391-411.

Vlček, V., Horáček, J., Luxa, M. & Veselý, J. (2008) Visualization of unsteady flow around a vibrating profile, in: *9th International Conference on Flow Induced Vibration FIV2008*, Praha, 30.6.-3.7.2008, Flow-Induced Vibration (eds. Zolotarev, I. & Horáček, J.). Praha: Institute of Thermomechanics, Academy of Sciences of the Czech Republic, v. v. i., -pp. 531-536. ISBN 80-87012-12-7.

Wilcox D.C. (1993) *Turbulence modeling for CFD*. DCW Industries.